Manufacturing Rev. **6**, 11 (2019)

https://doi.org/10.1051/mfreview/2019011

Special Issue - Advances in Research in New Forming Technology - from the ICNFT2018
Sybille Friedrich, Thomas Seefeld and Frank Vollertsen (Eds.)

Manufacturing Review
Available online at:
https://mfr.edp-open.org

RESEARCH ARTICLE OPEN ACCESS

Lubricant-free deep drawing using CO_2 and N_2 as volatile media injected through laser-drilled microholes

Ehsan Zahedi[1], Christoph Woerz[2], Gerd Reichardt[2,*], Georg Umlauf[3], Mathias Liewald[2], Jakob Barz[3], Rudolf Weber[1], Daniel J. Foerster[1], and Thomas Graf[1]

[1] Institut für Strahlwerkzeuge, University of Stuttgart, Pfaffenwaldring 43, 70569 Stuttgart, Germany
[2] Institute for Metal Forming Technology, University of Stuttgart, Holzgartenstrasse 17, 70174 Stuttgart, Germany
[3] Fraunhofer Institute for Interfacial Engineering and Biotechnology, Fraunhofer IGB, Nobelstraße 12, 70569 Stuttgart, Germany

Received: 14 December 2018 / Accepted: 24 April 2019

Abstract. Most metal forming processes use lubricants based on mineral oils as an intermediate medium to reduce friction and wear. To avoid the well-known drawbacks of oil lubrication, a novel and environment friendly lubrication system for deep-drawing processes was demonstrated at the University of Stuttgart. Liquid carbon dioxide and gaseous nitrogen are being used as volatile lubrication during the deep-drawing process, locally injected at high pressure through laser-drilled microholes. This new tribological system provides a significantly enlarged working range and at least 15% larger drawing depths compared to conventional oil lubrication.

Keywords: Deep drawing / laser micro machining / drilling

1 Introduction

In metal deep-drawing, usually mineral oil- or wax-based lubricants are used. These lubricants may contain toxic additives, and the formed components have to be cleaned in subsequent process steps in a cost and time-consuming manner [1]. To avoid these issues, a novel tribological system for sheet metal deep drawing that eliminates the use of conventional lubricants was developed at the University of Stuttgart. A sketch of the process is shown in Figure 1.

During the forming of the material, liquid CO_2 or N_2 is supplied at high pressure through diffusor-shaped, laser-drilled microholes. The liquid gas that evaporates close before or in the contact zone between sheet metal and tool surface, serves as lubricant, and subsequently evaporates without residue.

This paper summarizes the results achieved in the three basic contributions from the institutes involved. This includes (1) the flow behaviour of N_2 and CO_2 for different hole geometries, (2) the basic issues for laser drilling of shaped deep microholes, and (3) fundamental deep drawing tests with rectangular cups to demonstrate the capability of volatile lubricants. A CAD-drawing of a cross section through the segmented die of the deep drawing tool is shown in Figure 2.

2 Properties of CO_2 and N_2

Since the beginning of the 90s, the use of carbon dioxide as a working medium in refrigeration, air conditioning and heat pump processes has become the focus of technical interest. While in the chemical industry CO_2, was used as industrial gas as raw material, in the meantime it is also used as protective gas for packaged food, as fertilizer or for the production of medicine. Finally, in the late 1990s, the discussion on atmospheric greenhouse gas emissions in general and the capture, transport and storage of carbon capture and storage (CCS) in particular became more important. This puts carbon dioxide into the centre of technical and political interest.

First of all, another aspect will be briefly discussed: the danger potential associated with the large-scale handling of carbon dioxide. It is well known that carbon dioxide can be toxic and heavier than air. In the past, this has repeatedly resulted in fatal accidents in cellars or feed silos. In fact, the standard density (density at $T_n = 273.15\,\mathrm{K}$ and $p_n = 0.10\,\mathrm{MPa}$) of carbon dioxide is $\rho_n = 1.97\,\mathrm{kg/m^3}$. CO_2 is 1.529 times heavier than dry air. However, a dangerous accumulation of escaping carbon dioxide is usually limited to poorly ventilated rooms or cellars. Outdoors, mixing with the moving ambient air takes place quickly. CO_2 is not toxic only by the displacement of atmospheric oxygen, as a metabolite of the body, it also has an immediate effect on vital functions. It should be noted that although the maximum workplace concentration for carbon dioxide is

* e-mail: gerd.reichardt@ifu.uni-stuttgart.de

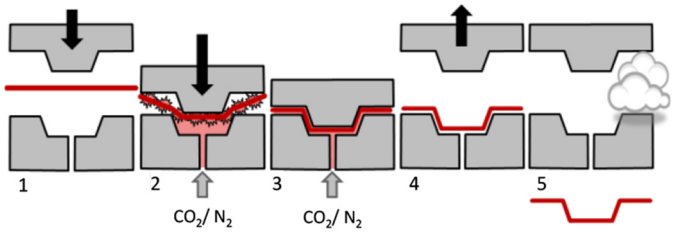

Fig. 1. Sketch of the forming process using volatile fluids as lubricant.

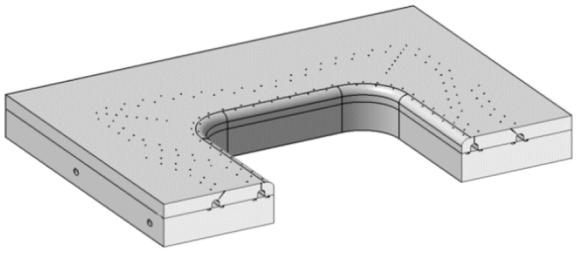

Fig. 2. Cross section through the segmented die of the deep drawing tool.

already reached at 0.5% (based on the partial pressure), only concentrations above 20% are lethal in the short-term. While gaseous CO_2 dissolves only a few substances, the solution behaviour improves in the liquid and especially in the supercritical state.

Figure 3 shows the p–T diagram of CO_2 and N_2. Along the sublimation curve, solid and gas exist simultaneously. Solid and liquid phases exist simultaneously along the melting curve. The sublimation and melting curves coincide with the vapour pressure curve. At the triple point, all three states of matter are gaseous, liquid and firmly in equilibrium [2,3]. At the upper end of the vapour pressure curve is the critical point. This point is characterized by the critical temperature T_k and the critical pressure p_k. If the temperature and the pressure are increased beyond the critical point, the pure substance is in the supercritical state.

In contrast, for nitrogen, the critical point is given for a temperature of 127.15 K and a pressure of 3.39 MPa. This requires that only a strong decrease in temperature at atmospheric pressure can liquefy N_2. A large increase in pressure above 3.39 MPa causes a transition to the supercritical region. In this area, the gas and liquid phases can no longer be separated. In addition, both properties of the states of aggregation are present in parallel. The supercritical state is as dense as a liquid but has the same viscosity as a gas.

Due to the numerous phase transitions in the working window from 1 bar to 60 bar, CO_2 is examined more closely. Nitrogen is in the gaseous state at any point in the processing chain (Tab. 1).

For these experiments, a pressurised gas cylinder filled with CO_2 at 6 MPa (60 bar). Due to the different densities, the lighter gas phase is above the liquid phase. The gas cylinder is equipped with a riser to insure the withdrawn

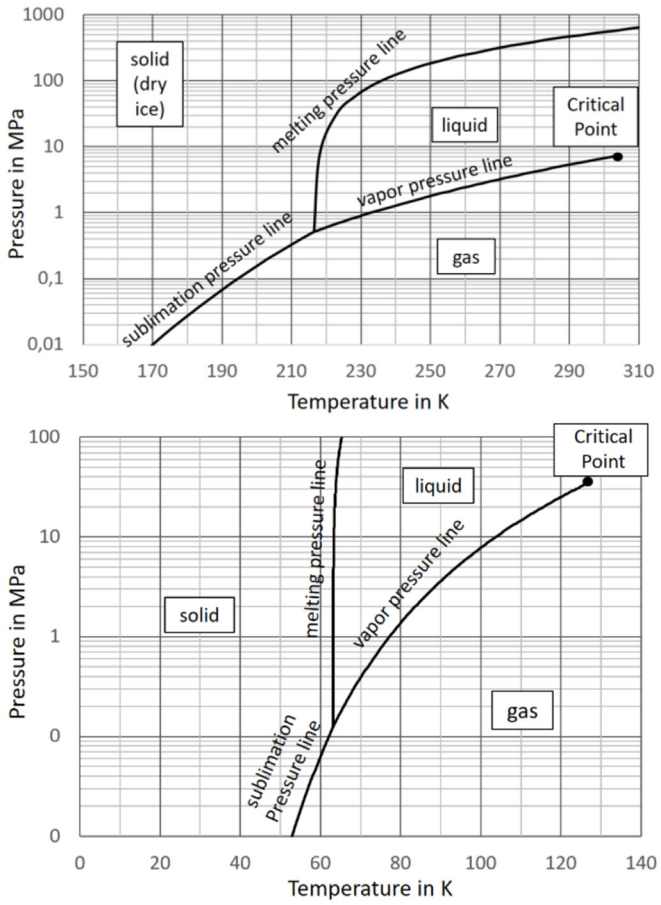

Fig. 3. p–T diagram for CO_2 (upper) and N_2 (bottom), according to [4,5].

Table 1. Comparison of physical properties of CO_2 and N_2.

Property	Value for CO_2	Value for N_2
Crit. temperature (K)	304.13	126.19
Crit. pressure (MPa)	7.37	3.39
Crit. density (kg/m^3)	467.60	313.30
Triple point temperature (K)	216.59	63.15
Triple point pressure (MPa)	0.52	0.01

CO_2 is in the liquid state during the whole period of consumption. During consumption, the liquid CO_2 flows through the riser upwards, through the leads and the microholes directly into the forming tool. The microholes are open towards atmosphere. By exiting through the holes, CO_2 expands and evaporates. As the evaporation process consumes heat (enthalpy of evaporation $\Delta H_{vap} =$ 574 kJ/kg @ 1013 hPa), the gas is cooled down and portions of it resublime and form so-called dry ice. This solid form of CO_2 can be seen very well by the whitish

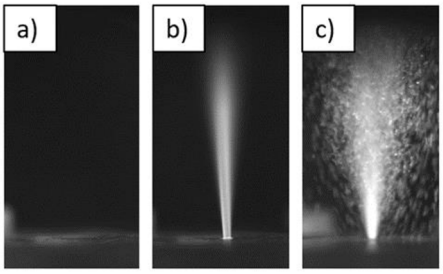

Fig. 4. Comparison between the aggregate states gaseous (a), solid (b) and liquid (c) during the flow out of CO_2 through a laser-drilled microhole.

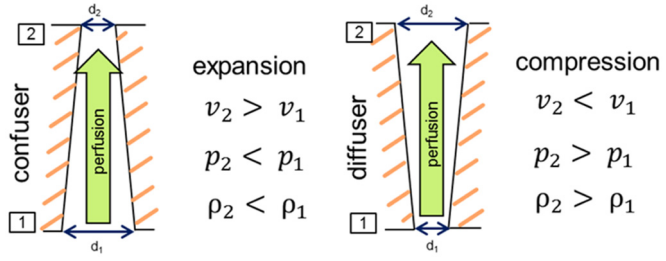

Fig. 5. Comparison between confuser and diffusor.

colour as shown in Figure 4. At this point, the temperature is 195 K. Further cooling of the gaseous part occurs during gas expansion by the Joule-Thomson effect: For CO_2, the substance-specific Joule-Thomson coefficient at ambient conditions is 1.1 K/bar [5]. At further distance, the solid portion of CO_2 sublimates: liquid CO_2 is not stable at atmospheric pressure, so the dry ice directly converts into gaseous CO_2.

The expansion at the microhole is supposed to take place adiabatically, i.e. without heat transfer to the surrounding material inside the microhole. Nozzle shapes are generally divided into two types of geometry, a confusor and a diffuser. The diffusor gradually widens its cross section in flow direction, the confusor becomes narrower (see Fig. 5).

Previous investigations (strip drawing tests) have shown that a diffuser shaped geometry with $d_1 = 200\,\mu m$ and $d_2 = 600\,\mu m$ is the optimum geometry. The microholes were drilled with an ultra-short pulsed laser in order to allow arbitrary shaping of the holes according to the needs described before. However, drilling of very deep microholes with the laser is not yet established and requires special attention due to basic physical limits which determine the resulting quality.

3 Basic laser drilling limits

One of the major reasons for reduced quality during laser processing with ultra-short laser pulses is the so-called heat accumulation [6,7]. In addition, the limited pulse energy limits the maximum drilling depth: With increasing hole depth, the total surface area of the wall of the microhole increases. This means that the average laser fluence (i.e. the laser pulse energy divided by the wall surface area) decreases. If the average fluence reaches the ablation threshold fluence, only very slow and localized drilling can occur. This limit is called "quality depth limit" in the following.

Table 2. Properties of the IFSW kW-class-ps laser system and the helical drilling optics.

IFSW kW-ps laser [7]	
Pulse duration	8 ps
Wavelength	1030 nm
Average power	≤650 W
Max. pulse energy	≤2.2 mJ
Repetition rate	≤300 kHz
M^2	<1.3
Polarization	Linear
Collimated beam diameter	5.2 mm
Helical drilling optics (GL-Trepan, GFH GmbH)	
Rotation speed	0–30 000 rpm
Hole diameters	0–1500 µm
Inclination angle	0–4°
Focusing and ablation threshold	
Focal length	400 mm
Focus diameter	140 µm
Polarization	Circular
Focus position	On the surface
Max. fluence	15 J/cm^2
Ablation threshold (steel, 8 ps, 1030 nm)	0.1 J/cm^2

Heat accumulation and the quality depth limit were investigated for the required geometry of the microholes. For the experiments, the prototype kW-class ps-laser of the IFSW was used [8]. The passive disk-amplifier of this laser allows very high pulse energies which are necessary for laser drilling of deep holes. The diameter of the holes was adjusted with a helical drilling optics. This optics moves the beam on a circle with adjustable diameter. Furthermore, the optics allows adjusting the inclination angle of the beam relative to the surface which is necessary for longitudinal shaping of the microholes. The properties of the laser, the helical drilling optics, and the focusing optics are summarized in Table 2.

As it is described in Section 2, the inlet and outlet diameters of the microholes have to be 600 µm and 200 µm. Drilling microholes with a specific geometry needs precise moving of the laser beam. A laser drilling optic assists to fulfil this task. To drill the needed hole geometries, the GL Trepan optics from GFH GmbH, Germany, was used. The principle of a laser-drilling optic is described in [10].

3.1 Heat accumulation

Heat accumulation was identified as one of the major quality-reducing effects for deep-hole drilling [6,7].

The laser system described above was used to determine the limits where heat accumulation effects

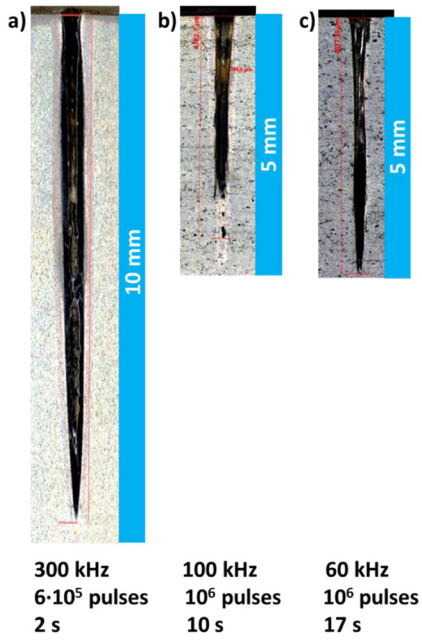

Fig. 6. Cross-sections of laser-drilled microholes with a pulse energy of 2.2 mJ. All samples were etched with Nital 5% for 40 seconds.

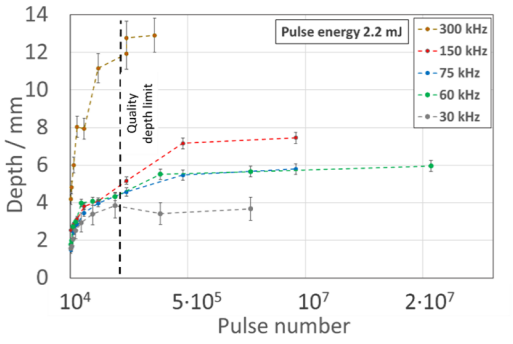

Fig. 7. Hole depth as a function of the number of pulses for the pulse energy of 2.2 mJ for different repetition rates.

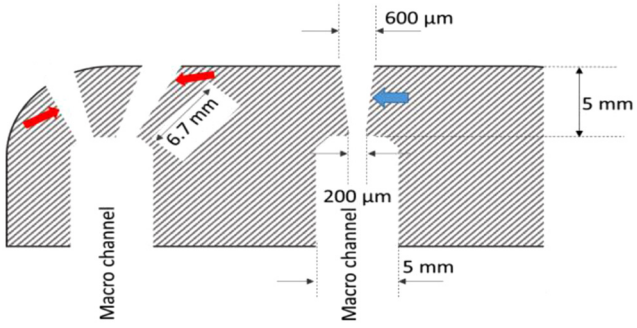

Fig. 8. Geometry and position of the microholes: depth of 5 mm for perpendicular (assigned with blue arrow) and depth of 6.7 mm for angled microholes (assigned with red arrows). The microholes are connected to the macro channel, which were manufactured by conventional mechanical tool.

begin to reduce the quality. The optically measurable occurrence of phase transitions in the material was defined as an indicator for a reduced quality. These phase transformations include the formation of to melt ($T \approx 1500\,°C$) as well as a solid phase transformation ($T \approx 950\,°C$). While the formation of melt is visible on the sample surface, the solid state phase transformations were analyzed by polishing and etching of the cross sections with Nital 5% for 40 s.

Figure 6 shows the effect of a decreasing repetition rate on the heat affected zone and the drilling progress for a constant pulse energy of 2.2 mJ. At 300 kHz and an average power of 660 W, the depth of the microhole was about 8 mm after 5×10^5 pulses (2 s of drilling time) (Fig. 6a). However, a large heat-affected zone of about 1 mm can be seen. If the repetition rate is reduced to 100 kHz (which leads to an average power of 220 W), the hole depth after 10^6 pulses (10 s of drilling time) was reduced to about 5 mm. A heat affected zone is still visible as a bright area along the walls of the hole and in particular in the bottom of the hole (Fig. 6b). Further reducing the repetition rate to 60 kHz yielded the same hole depth of about 5 mm after 10^6 pulses (17 s of drilling time) but without a visible heat affected zone and good hole quality.

These results lead to the conclusion that 60 kHz is the limiting frequency at the pulse energy of 2.2 mJ to maintain high quality of the drilled holes.

It is worth to mention that when drilling with a repetition rate of 300 kHz, melt ejections dominate the drilling process, leading to a higher drilling rate (depth per time). At the same time, melt ejections lead to a reduced quality of the hole [6,7].

3.2 Depth limit

The hole depth as a function of the number of laser pulses for different repetition rates is shown in Figure 7. The pulse energy was 2.2 mJ.

The drilling progress is very similar for repetition rates of 150 kHz and below. In the beginning of the drilling process, up to about 1×10^5 pulses, the drilling progress is very fast down to a depth of about 4 mm. As the depth increases, the process becomes slow and irregular. The faster drilling progress for $>2 \times 10^5$ pulses for the frequencies >30 kHz suggests, that heat accumulation gains influence after a very large number of pulses. It can be concluded that the above-mentioned "quality depth limit" is reached at about 4 mm for pulse energies of 2.2 mJ (marked by the dashed line in Fig. 7).

4 Laser drilling of microholes in the deep-drawing tool

4.1 Requirements

A sketch of the required geometries of the microholes are shown in Figure 8. The required hole depths and angles of the holes with respect to the surface of the deep drawing tool can be seen. The depth of the holes was either 5 mm or 6.7 mm, depending on the position of the hole inside the

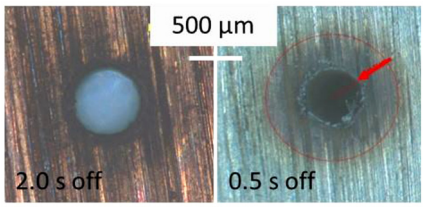

Fig. 9. Decreasing the break between the drilling intervals of 0.5 s from 2.0 s to 0.5 s results in the appearance of dross on the surface of the sample, marked by the red arrow.

tool. The angle of the hole relative to the tool surface was either perpendicular or 35°. In total, 254 microholes were drilled.

As the required depth exceeded the above-discussed quality depth of 4 mm, a higher number of pulses needs to be applied in order to drill through. Inevitably, the additional amount of energy is deposited into the capillary. To minimize the risk of damage, an additional break time was applied to the drilling strategy to optimize the hole quality: After drilling for 0.5 s, a break was introduced. The required duration of the break was determined experimentally. Figure 9 shows that decreasing the break between the drilling intervals from 2.0 s to 0.5 s results in the appearance of dross around the hole on the surface of the sample, marked with a red arrow.

4.2 Laser-drilled microholes

Based on the results of the basic investigations described above, the microholes in the deep drawing tool were drilled with 60 kHz, the maximum available pulse energy of 2.2 mJ, and the above-mentioned drilling strategy of a 0.5 s drilling interval follow by a 2.0 s break (for the depth of 6.7 mm). In Figure 10, typical cross-sections of the laser-drilled, deep microholes suitable for the deep drawing application are shown.

The net drilling time was 60 s and 320 s for the 5 mm and the 6.7 mm holes, respectively. Although the depth of 6.7 mm was reached, the respective drilling time was very long. That the quality depth limit was exceeded manifests in the longitudinal shape of the hole as seen in Figure 10. Down to a depth of about 4 mm (marked with a red arrow), the shape is conical and very regular. This depth corresponds to the "quality depth limit" as described above. For depths larger than 4 mm, the longer drilling time lead to an irregular widening of the hole cross-section. However, the holes were free of heat affected zones and free of burr on the surface. Overall, the quality was acceptable for the deep drawing experiments.

4.3 Manufacturing of the deep drawing tool

The complete deep drawing tool after production is shown in Figure 11.

Due to constraints of the micro-processing station, positioning of the blank with respect to the absolute coordinates of the holes and the angle relative to the surface was done manually using auxiliary tools. This caused in particular inaccuracy of the focus position relative to the surface of the blank, which resulted in a scattering of the hole diameters of about ±15%.

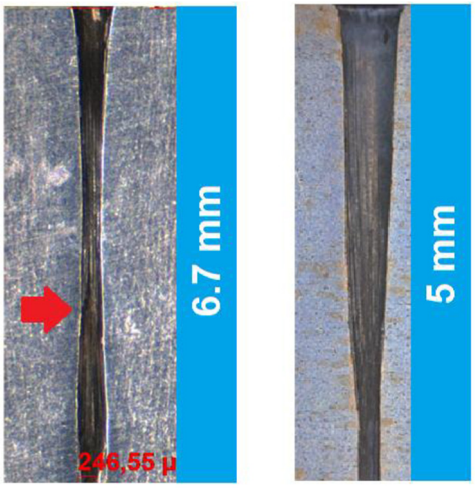

Fig. 10. Typical cross-sections of the laser-drilled, 6.7 mm (left) and 5 mm (right) deep microholes for the deep drawing application. The red arrow indicates the "quality depth limit".

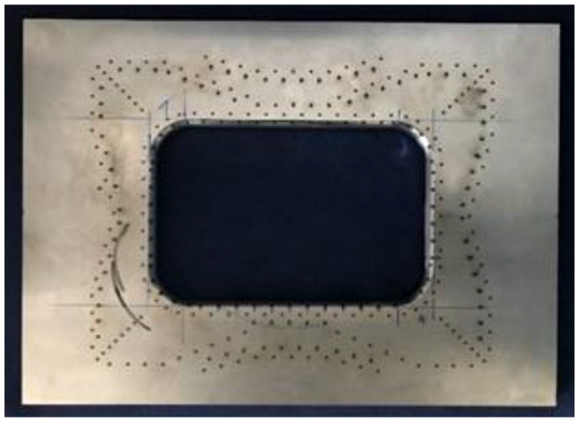

Fig. 11. Processed deep drawing tool.

4.4 Preparation of tool inserts for deflected strip drawing investigations

In order to further optimize the deep drawing process, additional experiments were prepared after the production of the forming tool. In preparation for the deflected strip drawing test, which is explained in Section 5.3, a tube with 11 micro holes needed to be produced. For this, an ultrashort pulsed laser (Spectra Physics Spitfire), providing pulses with an adjustable pulse duration between 35 fs and 10 ps at a maximum pulse energy of 7 mJ was used. As basis for the experimental design, the model presented in [9] was used. The pulse duration was set to 1 ps, while the used energy was set to 3 mJ for the percussion drilling experiments. For focusing, a lens with a focal diameter of 780 mm

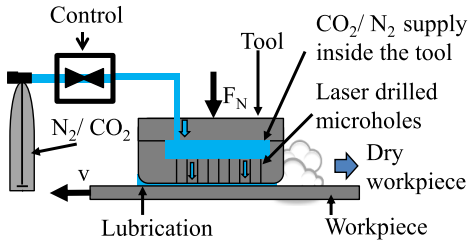

Fig. 12. Experimental setup of flat strip drawing test using volatile media.

was used, resulting in a focal diameter of 100 µm. The experimental findings according to the deflected strip drawing tests are given in Section 5.3.

5 Strip drawing investigations

5.1 Experimental setup of flat strip drawing investigations

In order to evaluate the lubricating effect of gases during deep drawing, a strip drawing testing rig was modified to determine the coefficient of friction under different conditions in such a way that the fluid could be introduced into the contact zone between the tool and the workpiece via laser-drilled microholes, which were inserted into strip drawing jaws, as it is shown in Figure 12.

With the help of this test rig, various parameter combinations, such as nozzle type, borehole arrangement, borehole diameter, contact normal pressure, drawing speed and fluid pressure could be investigated for their influences. For all executed flat strip drawing investigations electrolytic galvanized sheet material DC05 was used. Carbon dioxide in the conventional gas cylinder is present in a 2-phase state, where gaseous and liquid CO_2 are present at the same time. CO_2 is taken out of a standard gas bottle in its liquid state, so that the pressure cannot be adjusted and remains constant depending on level of exit temperature. The pressure of nitrogen is set to the same level as for carbon dioxide at the supply valve ($T = 20\,°C$, $p \approx 60$ bar) to maintain comparability.

The flat strip drawing test is an experimental setup to investigate the influence of different parameters on the friction coefficient. However, the elastic and plastic deformations of the sheet metal material that occur in the actual deep-drawing process (e.g. thickness reduction) cannot be reproduced. Nevertheless, this experiment is suitable to determine the qualitative influences of the individual parameters.

5.2 Results of flat strip drawing investigations

In order to gain a better understanding of the interdependencies of the tribological system using volatile media as lubricant substitutes, a large number of parameters were investigated [10,11]. The following gives a compact overview of the results obtained from the flat strip drawing experiments.

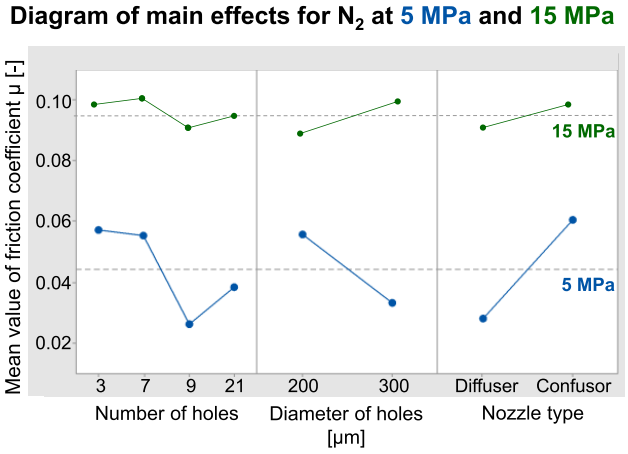

Fig. 13. Main effects on coefficient of friction μ determined with strip drawing investigations at 5 MPa (lower, blue values) and 15 MPa (higher, green values) surface pressure, drawing speed 100 mm/s, lubrication medium N_2. All values represent averaged values for the respective configurations [12].

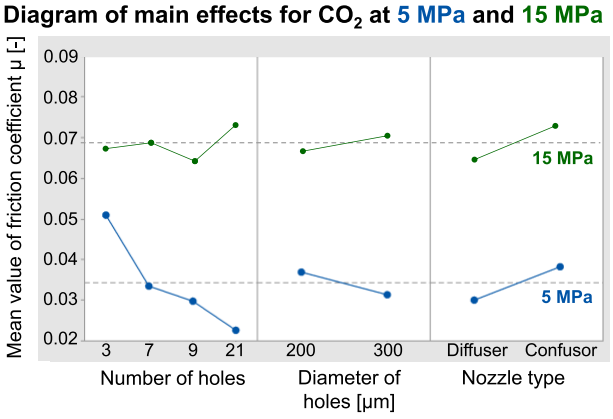

Fig. 14. Main effects on coefficient of friction μ determined with strip drawing investigations at 5 MPa (lower, blue values) and 15 MPa (higher, green values) surface pressure, drawing speed 100 mm/s, lubrication medium CO_2. All values represent averaged values for the respective configuration [12].

The effects of number of conical holes (3, 7, 9, 21) and the diameters of (200 µm, 300 µm) and nozzle types (diffuser, confuser) were investigated. The main effects of these parameters on the coefficient of friction are depicted in Figures 13 and 14.

Using nitrogen (N_2) or carbon dioxide (CO_2) as lubricant results in a significant reduction of the friction coefficient at low contact pressure (5 MPa) with an increasing number of bore holes. In the tests with 21 holes using N_2, friction slightly increases again, which can be justified by the fact that the pressure in the supply channels decreases sharply due to the increased outflow of the gas with a large number of holes and therefore a lubricating effect is only achieved in a weak manner. CO_2 is not that sensitive on the diameters of the supply channels, because the specific volume increase at 20 °C, is nearly fourfold due

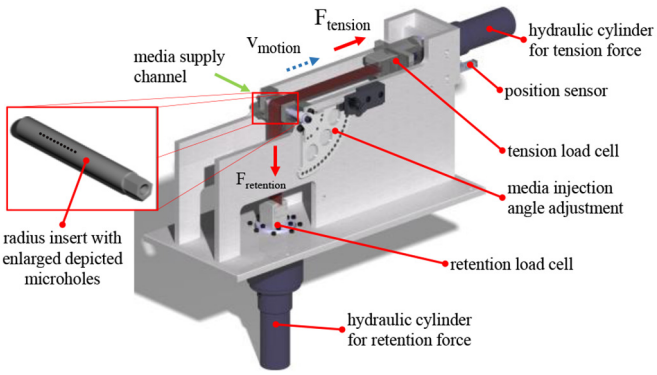

Fig. 15. Design of the testing rig for deflected strip drawing experiments [14].

to the phase change from liquid to gaseous. That's why decreasing pressures in the supply channels will occur at markedly higher output rates of CO_2 compared to N_2.

For both fluids, diffusors obtain lower friction coefficients compared to confusors at 5 MPa as well as at 15 MPa. This result was used, among all the experiments, for the design of the forming tool of the rectangular cup and so there all laser-drilled microholes were drilled as diffusers [13].

Dashed lines in both diagrams represent the averaged value of all friction coefficients obtained by strip drawing experiments at a contact pressure of 5 MPa and 15 MPa. As can be seen in the diagrams, CO_2 achieves lower averaged friction values than N_2 at both high and low surface pressures. A possible explanation of this effect could be the formation of dry ice. To get a better understanding of these effects, further investigations on the effects of dry ice formation when using CO_2 as a lubricant substitute [11] and the pressure conditions in the tool contact zone [13] were carried out in the course of this research work.

5.3 Experimental setup of deflected strip drawing investigations

Tool radii are one of the highest loaded zones of deep drawing tools regarding normal surface pressure. As mentioned before, flat strip drawing investigations do not take bending and stretching effects of the sheet metal strip into account. To get a deeper knowledge of friction conditions at high loaded tool radii and to overcome mentioned deficits, a deflected strip drawing testing rig was developed.

The design of the deflected strip drawing testing rig (cf. Fig. 15) is based on the conventional flat strip drawing testing rig. However, the sheet metal strip is deflected using a radius insert and is stretch-bent around a radius insert enclosing an angle of 90°. In this manner, the effects of plastic material elongation caused by the drawing process can also be taken into account. The drawing velocity of the sheet metal specimens is kept constant during the experiments and can be determined using an integrated displacement sensor. Occurring tension force and restraining force are measured by using two piezo load cells. Different normal surface pressures between specimen and tool surface can be set by varying the retention force.

The obtained values of the coefficient of friction at the radius insert were calculated from the measured restraining and tension forces using the analytical calculation of conventional rope friction according to Euler and Eytelwein [15]. The bending influence of the sheet metal strip on the acting forces was neglected, as these forces are negligibly small within the sheet metal material investigated (DC05 + ZE, deep-drawing steel grade with a sheet thickness of 0.7 mm).

The used radius inserts were designed with a feeding channel for the volatile media. In the contact area between the sheet metal strip and the radius insert, laser drilled microholes were integrated for the feeding of the medium. These allow injecting the lubricant into the friction zone. These microholes were arranged in one single row and are evenly distributed for first experiments. As determined in the preliminary in-vestigations, diffuser-shaped microholes lead to low coefficients of friction [13]. For this reason, only diffuser-shaped microholes were used for these investigations. In order to investigate the influence of the injection angle on the tribological conditions at the tool radius inserts, an angle adjustment was integrated into the testing rig for positioning the microholes in the 90° enclosed angle (see Fig. 15). Doing so, the optimum injection angle for the introduction of the volatile lubricant could be determined.

5.4 Results of deflected strip drawing investigations

Presented results were gained by investigations using CO_2 as volatile lubricant. The carbon dioxide was taken from a standard gas cylinder with a riser so that CO_2 in a liquid state could flow into the radius insert at approximately 60 bar (6 MPa, at a temperature of 20 °C). The expected phase change into gaseous state takes place shortly before leaving the diffuser shaped microholes. Investigations using N_2 as lubricant substitute are ongoing.

In order to vary the surface pressure at the radius insert, the restraining force was adjusted to four different levels (3.4 kN, 4 kN, 5 kN and 6.1 kN). Also the injection angle α was varied in 3 steps (30°, 45° and 60°).

The repeatability of these experiments showed quite small fluctuations in terms of measured values of less than 2% across all parameters combinations. Only when adhesions on the radius inserts occurred, the fluctuations of the friction values increased significantly (compare Fig. 16, injection angle of 30°).

Setting the injection angle to $\alpha = 45°$, a mean friction coefficient of $\mu = 0.26$ could be determined when applying a retention force of 3.4 kN. At a retention force of 6.1 kN, a friction value of $\mu = 0.19$ was measured on average. The descending trend of the series of curves in figure at an injection angle of 30°, 45° and 60° to almost the equal value of friction at $F_r = 6$ kN ($\mu = 0.19$) is remarkable. This means that for high retention forces and therefore for high surface pressures the injection angle does not show any influence on the friction behaviour. Also notable is the fact that for high retention forces lowest coefficients of friction were measured. A plausible explanation for this special behaviour is the sealing effect for gaseous lubricants and the corresponding static counterpressure of used volatile

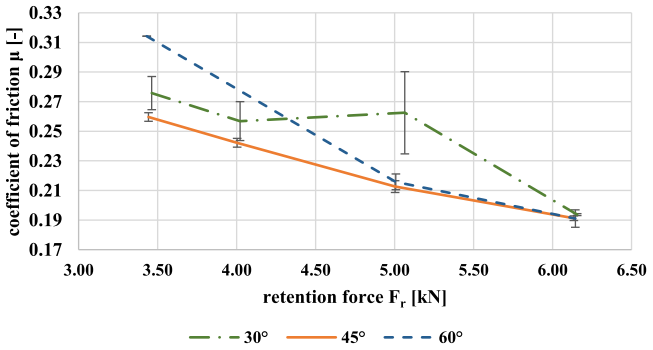

Fig. 16. Coefficient of friction for a radius insert of 5 mm radius using CO_2 as lubricant substitute at different injection angles α (30°, 45°, 60°) [15].

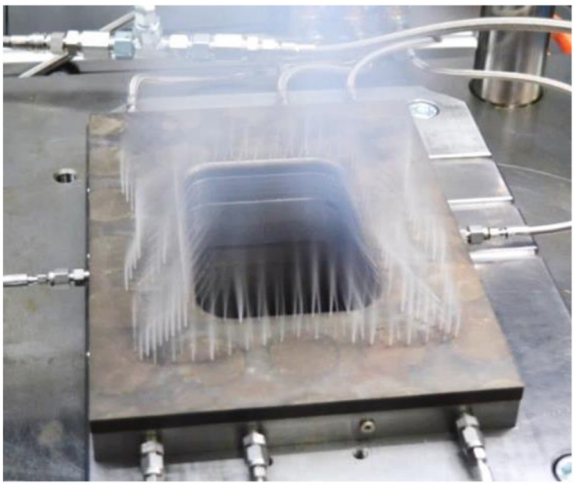

Fig. 17. Free flow out of the CO_2 through laser-drilled microholes in the die of the deep drawing tool.

(gaseous) media in the gap between tool and specimen surface. The same behaviour was found in [16] for a conventional lubrication system. Similar to this sealing effect between specimen and tool surface using volatile lubricants, the occurrence of static counter pressure using conventional liquid lubricants causes this behaviour.

Another notable observation was made concerning the occurrence of adhesion onto the tool radius. For injection angles of 30° and lower, medium retention forces as well as adhesions occurred during the drawing process at the tool radius. As adhesions occur not exactly in the same way in every repeated experiment, measured fluctuations of the coefficient of friction were significantly increasing.

Despite the already achieved reduction of friction at high surface pressure levels, the results suggest that the friction at radii have to be reduced compared to the significantly lower friction values in flat strip drawing tests (cf. Fig. 16 with 13 and 14). This aim ensures stable forming processes and low tool wear. Further investigations on the optimization of the injection angle indicate that lowest friction values can be obtained setting the injection angle between 40° and 45°.

6 Dry deep drawing of a rectangular cup

6.1 Tool design

In order to reduce the drilling depth for the laser process without reducing the tool strength, a segmented tool design was chosen (see Fig. 2). The base plate contains the holes for the media supply and a sealing to avoid an uncontrolled flow out between the plates while the upper plate contains different supply channels and laser-drilled microholes. The position of the supply channels determines the location of microholes. In order to avoid a free flow out of the media through the microholes at the end of the forming process, the position of the supply channels was optimized using a sheet metal forming simulation of the blank draw-in. As a result, one ring channel was integrated next to the die radius and four additional channels were arranged with regard to the blank draw-in. Each supply channel could be controlled separately by a valve to stop free flow out of media during deep drawing.

One row of microholes was drilled perpendicular into the supply channel having a depth of 5 mm, while another row was incorporated by an angle of 35° and a depth of 6.7 mm. Additional microholes were placed in the die radius area. In total, 154 microholes were distributed over the tool surface of the die. For the blankholder, the same design was chosen though without radius. Here about 100 microholes were drilled into the tool.

Due to some problems in the tool manufacturing, it was necessary to re-mill the die radius after laser drilling. For this purpose, the tool was connected to a compressed air system applying a pressure level of 2 bar during the milling process. By doing so, none of the microholes was blocked due to the machining process. Also after the final hardening process of the tool, no blockage of the microholes could be observed. The final assembly of the die tool is shown in Figure 17 while a free flow out of the CO_2 through the laser-drilled microholes is activated.

6.2 Experimental setup

In order to understand the limits of this new tribological system, several deep drawing tests have been carried out and compared with a conventional deep drawing process using mineral oil- or wax-based lubricants. An established method is the determination of the process window. Usually, the blank holder force and the drawing ratio is varied in the deep drawing process in order to find the maximum drawing depth without wrinkles or cracks. By doing so, the valid process window can be determined, where no cracks and no wrinkles in the flange area appear. For non-rotational parts the drawing depth is used instead of the drawing ratio.

All drawing experiments were carried out using electrolytic galvanized sheet material DC05. The sheets were cleaned manually and then decreased within an acetone bath in order to remove remaining oil on the sheet. Liquid CO_2 having an initial pressure level $p_{initial}$ of 60 bar and gaseous N_2 at the same pressure level were used as temporarily acting lubricant for dry metal forming. The

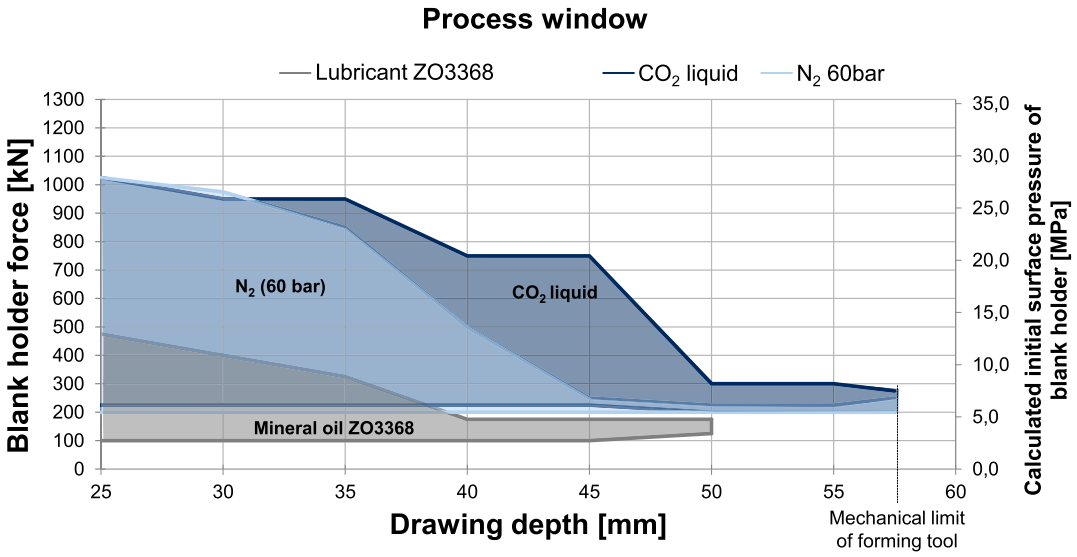

Fig. 18. Process windows for deep drawing of a rectangular cup using different lubrication systems [13].

supply of the media was controlled by the movement of the ram. The supply was switched on in the moment of the first contact between the tool and the sheet and shut down at the bottom dead centre of the press. Additionally, drawings with the lubricant Wisura ZO3368 (1.5 g/m^2) were investigated using the same tool. All tests were carried out on an AIDA servo press at a ram speed of 6 strokes per minute which corresponds approximately to 100 mm/s at the beginning of the forming process.

6.3 Experimental results and discussion

Presented approach for dry metal forming was tested successfully and a rectangular cup was deep drawn using N_2 and CO_2 as temporarily acting lubrication for the very first time. In accordance with former tests results investigating the coefficient of friction [12] and the deep drawing of a U-shaped profile geometry [11], the new lubrication system performed better than the conventional one using a mineral oil-based lubricant (see Fig. 18).

The maximum drawing depth could be increased to 57.5 mm by using CO_2 and N_2. This depth corresponds to the mechanical limit of the tool. By using lubricant ZO3368, only 50 mm as a maximum drawing depth was achieved. Also the fracture limit was raised by up to 50%, depending on the drawing depth by using CO_2 as well as N_2. Thereby, CO_2 performs better for deeper cups than N_2. It is assumed that this is caused by different pressure levels acting in the gap between the sheet and the tool, resulting from the use of different media [13]. In general this pressure in the gap p_{gap} is influenced by microholes (position, numbers, nozzle type), the initial pressure level of the injected media $p_{initial}$ and the sealing effect between tool surface and the sheet. Also the sealing effect is influenced by many factors such as the blankholder force $F_{Blankholder}$, the tool and sheet surface roughness and the thinning and thickening of part flange during deep drawing. Finally, there are interactions between the sealing effect, the pressure level p_{gap} and the height of the mean gap h_{gap}

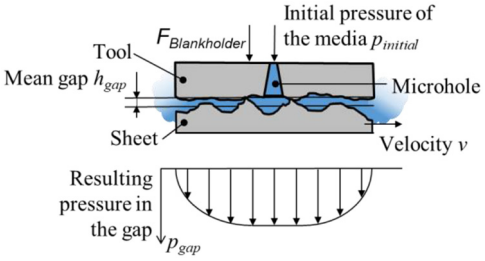

Fig. 19. Schematic illustration of the resulting pressure between sheet and tool.

between the sheet asperities and the forming tool. A schematic illustration of the conditions in the gap and the applied designations are shown in Figure 19.

When deep drawing with volatile media acting as lubrication, not only the fracture limit, but also the wrinkle limit was increased noticeably (cf. Fig. 18). This effect can be explained also by the assumption that the mean gap h_{gap} and the pressure p_{gap} mainly do influence the sheet metal forming behaviour. For lower blank holder forces a higher gap h_{gap} occur without or with minimum contact areas between the tool and the sheet asperities. While forming, wrinkles of 1st order develop due to increasing tension stress in the blank without prevention by the blank holder. Thereby, the pressure in the gap, which is a scalar quantity acting in all directions, cannot avoid the local development of wrinkles. The outflowing gas through the wrinkles additionally supports such development. Other tests indicate that the wrinkle limit is raised further by using a pressure $p_{initial}$ of N_2 higher than 60 bar. However, also the fracture limit can be increased significantly. This confirms the assumption that the resulting pressure level p_{gap} of the volatile media between the sheet and tool mainly influences the friction behaviour and therefore the forming limits in the deep drawing process of this new approach.

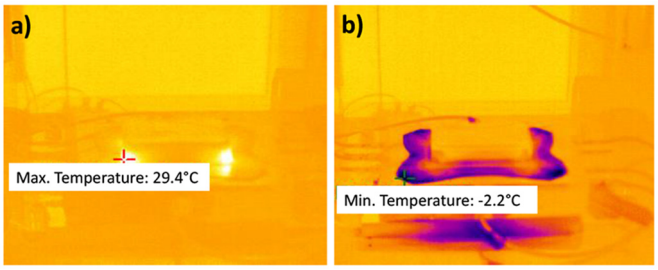

Fig. 20. Measured temperature on the sheet surface after deep drawing using (a) nitrogen and (b) liquid carbon dioxide as lubricant.

In addition to those investigations on process limits in deep drawing, the cooling effect on the sheet surface caused by the Joule-Thomson effect during the relaxation of CO_2 and N_2 was investigated. The temperature was measured visually after the deep drawing process using a thermal camera.

In Figure 20, the visualized temperature is shown using nitrogen (Fig. 20a) and liquid carbon dioxide (Fig. 20b) as lubricant for the same process at a drawing depth of 35 mm and a blank holder force of 275 kN. The maximum measured temperature (29.4 °C) after deep drawing using nitrogen is almost similar to the sheet temperature when using mineral oil-based lubricants (30.1 °C). The heating in the corner of the cup is caused by dissipating forming energy and friction heat. In contrast, using liquid CO_2 as temporally acting lubricant reduces the sheet temperature in the flange area down to −2.2°C (see Fig. 20b). Compared to the first deep drawing experiments using a U-profile geometry [11], a cooling of only a few degrees Celsius was measured. The cooling effect has a higher influence when deep drawing the rectangular cup. Additional to that, the control of the valves also plays an important role. Finding the right timing to switch on and off the flow of media appears to be more complex for the drawing process of a rectangular cup, having curved arrangements of microhole positions on the tool surface and a more complex draw-in compared to previously described drawn parts. Another reason might be given by a changing flange thickness during drawing, counteracting to the local blank holder force. Small gaps between the tool and the sheet induced by small wrinkles of 1st order can occur, supporting the outflow of the CO_2 and therefore the cooling of the sheet due to a high velocity of the media. According to these results, the flow control and also the position of the microholes have to be optimized in further research work in order to reduce an extreme cooling of the sheet. A different approach is to use the cooling effect actively to reduce the heating during drawing process, while a heating of parts due to friction heat and dissipating forming energy is undesirable.

However, the presented results show that dry forming by means of temporally acting volatile media is possible. This not only allows an equivalent substitution of mineral oil-based lubricants but also an enhancement of the process limits in sheet metal forming. Especially using nitrogen with a pressured level adjusted to the respective process conditions is extremely promising.

7 Conclusions

The progress in the use of volatile media as lubricant substitutes in the deep drawing process in this paper were demonstrated based on achieved results. Furthermore, numerous technological challenges in the manufacturing process of precise micro-drilling by laser drilling were mastered. Also deepened knowledge could be gained experimentally and numerically by examining emerging friction conditions within the tool contact zone. Furthermore, after deep drawing of approximately 300 cups under dry as well as lubricated conditions no microholes were blocked by zinc abrasion or other effects. It can be assumed that blockage of the microholes is not a limitation factor for this new approach. As a next step, these results will be confirmed by prospective deep drawing endurance tests. Further performed measures also will be implemented into the test stand in the coming funding period. Further tool radii of the new testing rig, which are subjected to high friction and wear loads, will be provided with feedholes for volatile media flow. Complex friction conditions in corner areas and interaction with deep-drawing process will be investigated in this special testing rig. A further goal of future research is to expand the range of applications for zinc-coated steel sheets to include selected aluminium sheet materials, which poses enormous challenges with regard to a more complex tribological system and its susceptibility to failure. Furthermore, the theoretical knowledge of the friction behaviour of volatile media in the tribological system will be further deepened in order to understand and specifically influence the occurring effects and thus to ensure robust and stable deep drawing processes.

The scientific investigations of this paper are funded by the German Research Foundation (DFG) within the priority program SPP 1676 Dry Metal Forming – Sustainable Production by Dry Processing in Metal Forming.

References

1. F. Vollertsen, F. Schmidt, Dry metal forming: definition, chances and challenges, IJPEM-GT **1** (2014) 59–62
2. P. Kapler, Partikelbildung und −morphologie bei der Hochdruckmikronisierung gashaltiger Lösungen, Dissertation, Ruhr-Universität Bochum, 2002
3. Fachlabor UTRM SoSe 2010, Hochdruckextraktion mit CO_2
4. P.W. Atkins, J. de Paula, Physical Chemistry, Oxford University Press, Oxford, 2014, 10th Revised Edition
5. ChemicaLogic Corporation, http://www.chemicalogic.com/Pages/DownloadPhaseDiagrams.html, 2018
6. R. Weber, T. Graf, P. Berger, V. Onuseit, C. Freitag, M. Wiedenmann, A. Feuer, Heat accumulation during pulsed laser materials processing, Opt. Exp. **22** (2014) 11312–11324, and Erratum thereto in Opt. Exp. **22** (2014) 28232
7. D.J. Förster, R. Weber, T. Graf, Residual heat during ultrashort laser drilling of metals, in *Proceedings of LPM 2017 – the 18th International Symposium on Laser Precision Microfabrication, Kitakyushu*, 2017
8. J.P. Negel, A. Voss, M. Abdou Ahmed, D. Bauer, D. Sutter, A. Killi, T. Graf, 1.1 kW average output power from a thin-

disk multipass amplifier for ultrashort laser pulses, Opt. Lett. **38** (2013) 5442–5445
9. D.J. Förster, R. Weber, D. Holder, T. Graf, Estimation of the depth limit for percussion drilling with picosecond laser pulses, Opt. Exp. **26** (2018) 11546–11552
10. G. Umlauf, E. Zahedi, C. Woerz, J. Barz, M. Liewald, T. Graf, G.E.M. Tovar, Grundlagen-untersuchungen zur Herstellung von Lasermikro-bohrungen in Stahl und dem Ausströmverhalten von CO_2 als Trockenschmiermedium, Dry Met. Forming OAJ FMT **2** (2016) 18–24
11. C. Woerz, E. Zahedi, G. Umlauf, M. Liewald, R. Weber, T. Graf, G.E.M. Tovar, Tiefziehen eines U-Profils mit flüchtigen Medien als Schmierstoffer- satz, Dry Met. Forming OAJ FMT **3** (2017) 50–61
12. C. Woerz, M. Liewald, M. Singer, Investigation of tribological conditions in the strip drawing test using liquid CO_2 and N_2 as a volatile lubricant, in *Proc. of 7th ICTMP*, 2016, pp. 140–148
13. C. Woerz, G. Reichardt, M. Liewald, E. Zahedi, R. Weber, T. Graf, Dry deep drawing of a rectangular cup assisted by volatile media injected from laser-drilled microholes, Dry Met. Forming OAJ FMT **4** (2018) 1–8
14. G. Reichardt, M. Liewald, Friction conditions on deep drawing tool radii when using volatile media as lubrication substitute, in *TMS 2019 – Supplemental proceedings*, 2019
15. G. Reichardt, M. Liewald, Investigation on friction behaviour of deep drawing radii using volatile media as lubricant substitutes, in *Proceedings of the 18th Conference on Sheet Metal, SHEMET 2019, Procedia Manufacturing, Leuven, Belgium*, 2019, pp. 193–200
16. A. Papaioanu, Einsatz eines neuartigen Verfahrens zum kombinierten Recken und Tiefziehen von Außenhauptbeplankungen aus Feinblech, Beiträge zur Umformtechnik 81, Dissertation, University of Stuttgart, Institute for Metal Forming Technology, 2016

Cite this article as: Ehsan Zahedi, Christoph Woerz, Gerd Reichardt, Georg Umlauf, Mathias Liewald, Jakob Barz, Rudolf Weber, Daniel J. Foerster, Thomas Graf, Lubricant-free deep drawing using CO_2 and N_2 as volatile media injected through laser-drilled microholes, Manufacturing Rev. **6**, 11 (2019)